Paper No.
12869

NACE INTERNATIONAL
CORROSION Conference & Expo 2019

A Modified Thermodynamic Model for the Prediction of Mild Steel Corrosion Product Formation at High Temperature in an Aqueous H_2S Environment

Shujun Gao, Bruce Brown, David Young, Srdjan Nesic, Marc Singer
Institute for Corrosion and Multiphase Technology,
Department of Chemical & Biomolecular Engineering, Ohio University
342 West State Street
Athens, OH, 45701
USA

ABSTRACT

The prediction of phase identity and characteristics of corrosion products formed on the corroding metal surface is of prime importance to understanding the corrosion mechanisms and the protectiveness conferred by the formed layers. Pourbaix diagrams, developed for CO_2 environments, are typically successful in predicting (depending on pH, steel potential, temperature, pCO_2, etc) the most stable forms of corrosion products. In H_2S environments, however, it is more difficult to build a representative thermodynamic model (Pourbaix diagram) due to the formation of various iron sulfide polymorphs and phases which is a strongly kinetically controlled phenomenon. In addition, high temperature studies have also shown that a thermodynamically less stable but kinetically favored inner Fe_3O_4 layer developed under the iron sulfide layer and greatly affected the corrosion rate. In this paper, experiments performed at high temperature at different partial pressures of H_2S (pH_2S=0.10~2.0 bar) were conducted to investigate polymorphous iron sulfide formation and determine if the inner Fe_3O_4 corrosion product layer would fully convert to iron sulfide if the right conditions were met. The results show that the Fe_3O_4 layer is not a transient corrosion product layer, as previously thought, since it was always present in all the experimental conditions tested. A modified thermodynamic model was proposed by reconsidering the Fe_3O_4 stability zone in the Pourbaix diagram. The current model shows better agreement with the experimental results because of these changes.

Key words*: hydrogen sulfide; high temperature corrosion, iron sulfide; Fe_3O_4, Pourbaix diagram*

INTRODUCTION

With the increasing demand of energy, the exploration of hydrocarbon in oil and gas industry has moved to deeper and deeper wells, which are frequently associated with high temperature, high pressure, and high sour gas content (H_2S). High temperature H_2S corrosion brings serious challenges to infrastructure integrity, materials selection, and corrosion mitigation.[1-8]

The effects of high temperature and exposure time on the H_2S corrosion kinetics and Fe_xS_y transformation sequence have been studied in previous work.[9-10] It was found that the formation of corrosion products was responsible for the initial rapid decrease in corrosion rates, which eventually stabilized over time at

high temperatures.[9] The observed formation and transformation sequence at high temperature was mackinawite → troilite → pyrrhotite → pyrite. With the increase of temperature (80°C~200°C) and time (1~21 days), iron sulfide transformed to more thermodynamically stable phases.[10] However, these tests were performed at a constant H_2S partial pressure (0.1 bar) and the effect of H_2S content (pH_2S) on the corrosion rate of carbon steel and iron sulfide transformation at high temperature has not been studied. Generally, H_2S plays a dual role. Firstly, it accelerates the corrosion rate by providing an additional cathodic reaction:

$$2H_2S(aq) + 2e^- \rightarrow H_2(g) + 2HS^-(aq) \quad (1)$$

Secondly, it favors the formation of an iron sulfide layer by providing more HS^- ions:

$$Fe^{2+}(aq) + HS^-(aq) \rightarrow FeS(s) + H^+(aq) \quad (2)$$

Sun, *et al.*,[11] stated that the corrosion kinetics governs the overall phenomenon in the low pH_2S range, while FeS layer formation plays a dominant role in the higher pH_2S range. Therefore, a maximum in corrosion rate can be observed when increasing pH_2S, all other conditions being constant. However, the exact pH_2S values were not reported in the paper. Other literature also showed that the increase of pH_2S could either cause an acceleration or a retardation of the corrosion rate, depending on pH_2S, pH, temperature, and exposure time.[12-15] However, the water chemistry in these tests was not specified or controlled and the types of corrosion products were not characterized. Moreover, all the above experiments were performed only at low temperatures, and the effect of high temperature is still unknown.

At high temperature, another significant difference is that an inner Fe_3O_4 layer can also form. Fe_3O_4 is thermodynamically less stable but kinetically favored at high temperature.[16] It was demonstrated that Fe_3O_4 forms continuously at the steel/Fe_3O_4 interface, and converts to FeS at the Fe_3O_4/FeS interface.[17] The conversion reaction is electrochemical and involves aqueous $[H_2S]_{aq}$:

$$Fe_3O_4(s) + 3H_2S(aq) + 2H^+(aq) + 2e^- \rightarrow 3FeS(s) + 4H_2O(l) \quad (3)$$

Therefore, it is very relevant to investigate to what extent the Fe_3O_4 conversion to FeS occurs and to determine if a complete conversion to FeS would happen with an increase of pH_2S.

The thermodynamic model (Pourbaix diagram) for an H_2S environment has been already developed and verified at low temperatures (< 80°C).[18] However, it does not take into account Fe_3O_4 formation as part of the corrosion product at high temperatures. Given that the presence of Fe_3O_4 can greatly affect the corrosion rate, it is important to reflect its presence accurately in the thermodynamic model at high temperatures.

In summary, three research objectives are identified:

1. Investigation of high pH_2S on corrosion rates and on corrosion product formation at high temperature.
2. Investigation of the extent of Fe_3O_4 to FeS conversion at different pH_2S at high temperature.
3. Update thermodynamic model (Pourbaix diagram) to reflect the presence of Fe_3O_4 corrosion product layer at high temperature.

In order to address the above mentioned three research questions, experiments with different pH_2S (0.10~2.0 bar) at 120°C were conducted. Linear polarization resistance (LPR), X-ray diffraction (XRD), scanning electron microscopy with energy dispersive X-ray spectroscopy microanalysis (SEM/EDS) were employed to investigate the corrosion kinetics and layer transformation/conversion. The previously constructed Pourbaix diagram was then revisited and rebuilt to meet the needs for these higher temperatures.

EXPERIMENTAL PROCEDURE

The H_2S experiments were performed in a 7 L Hastelloy autoclave as shown in Figure 1. A typical three electrode setup was employed to conduct electrochemical measurements. The working electrode was an API 5L X65 mild steel cylinder. The chemical composition of this tempered martensitic steel is shown in Table 1. A Pt-coated Nb cylinder served as the counter electrode and a commercially available high temperature, high pressure Zr/ZrO_2 pH probe was used as a pseudo reference electrode. It could be employed as a reference electrode as long as its potential was stable under the operating conditions, but the exact potential value was still unknown.[19] Square specimens made from X65 were suspended using a PTFE-coated 304 stainless steel string. A concentric impeller was rotated at 1000 rpm to keep the solution well mixed during each experiment. The testing electrolyte was deoxygenated 1% wt. NaCl.

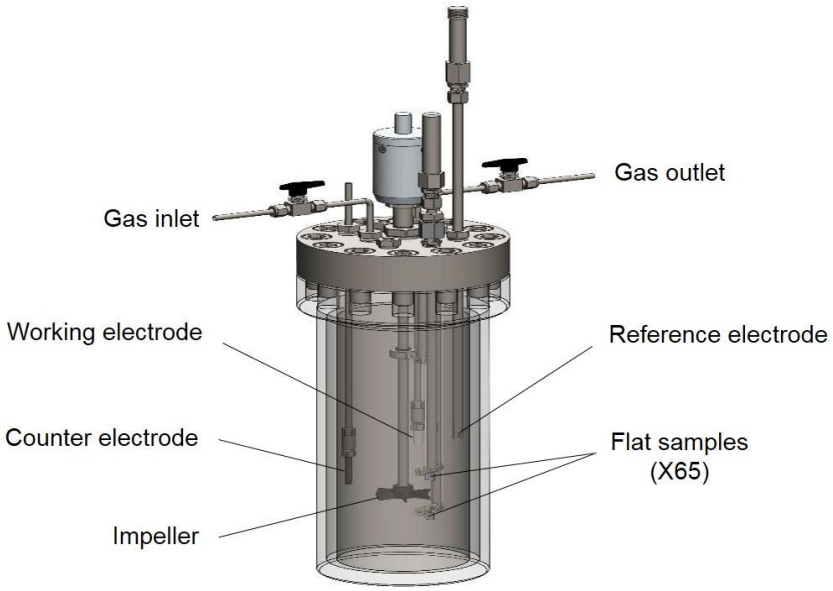

Figure 1 Experimental autoclave set up.

Table 1 Chemical composition of API 5L X65 carbon steel (wt%).

C	Mn	Nb	P	S	Ti	V	Fe
0.05	1.51	0.03	0.004	< 0.001	0.01	0.04	Balance

The aqueous speciation related to the different tested pH_2S was calculated according to an in-house water chemistry model developed for a closed system[16] and are summarized in Table 2. The pH at room temperature was adjusted according to the water chemistry calculations to achieve an initial pH of 4.0 and the target pH_2S (Table 2) when the temperature reached 120°C. It took approximately 30 min to heat the autoclave from room temperature to 120°C. LPR corrosion rate measurement was then conducted between -5 mV and +5 mV *vs*. OCP at a scan rate of 0.125 mV/s. After each experiment, the corroded specimens were retrieved and characterized XRD and SEM/EDS. Other experiment details can be found elsewhere.[16]

Table 2 Test matrix for the effect of pH_2S.

Parameter	Value			
Temperature, °C	120			
pH_2S, bar	0.10	0.50	1.0	2.0
$[H_2S]_{aq}$, mol/L	0.00385	0.01400	0.02800	0.05600
Initial pH	4.0			
Rotating speed, rpm	1000			
Duration, days	4			

RESULTS AND DISSCUSION

Effect of pH_2S

The measured corrosion rates obtained with different pH_2S at 120°C are shown in Figure 12. The error bars were determined from linear portions of repeated LPR measurements. There is no obvious trend for the initial corrosion rate (3~8 mm/y) probably due to the formation of relatively protective corrosion products before the autoclave reached the high testing temperature, especially at higher pH_2S. The formation of corrosion products is, however, inevitable for high temperature and high pressure tests since no adjustment can be made to control the conditions once the autoclave has been closed. After a few hours, the corrosion rates decreased quickly to a stable corrosion rate between 0.4 to 2 mm/yr. The stabilized corrosion rate tended to decrease with increasing pH_2S except at 1.0 and 2.0 bar H_2S. This was attributed to severe localized corrosion due to pyrite formation, which will be discussed later.

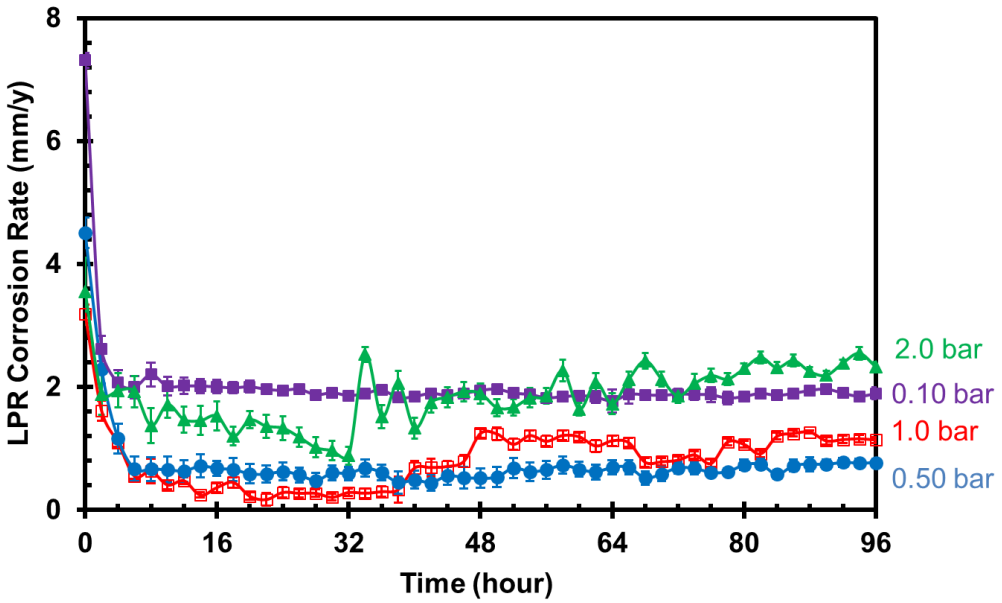

Figure 2. LPR corrosion rate at different pH_2S, T=120°C, initial pH=4.0, *B*=23 mV/decade.

Figure 3 shows the corrosion rate measured by weight loss which is compared with LPR time-averaged corrosion rate. The error bar for the weight loss is from three samples exposed in a single experiment. Good agreement can be observed at every studied pH_2S by using a *B* value of 23 mV/decade. This demonstrates that the general trend of LPR measurements is valid under these conditions. A minimum corrosion rate can be observed at 0.5 bar H_2S. However, larger deviations were observed at 1.0 and 2.0 bar. This is probably due to the corrosion mechanism and the resulting *B* value being altered by the different FeS layers formed on the surface.

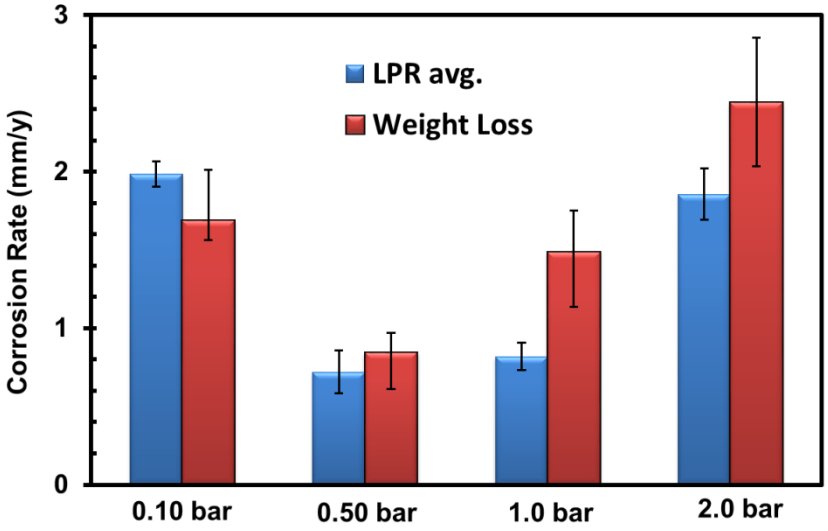

Figure 3. Comparison of corrosion rates measured by LPR average and weight loss at different pH_2S, T=120°C, initial pH=4.0, 4 days.

The corrosion product layers were characterized by XRD, as shown in Figure 4. The corresponding SEM images are shown in Figure 5 and Figure 6. At 0.10 bar H_2S, the main iron sulfide was identified as troilite (FeS) with a small amount of mackinawite (FeS). The elongated needle-like and flower-like troilite crystal morphologies can be seen in the SEM images. The same structure of troilite was also found in other studies.[20-22] Troilite transformed to pyrrhotite ($Fe_{1-x}S$, $0 \le x \le 0.17$) after increasing pH_2S to 0.50 bar. SEM images show the steel surface was fully covered by a dense layer of pyrrhotite crystals with a hexagonal flake-like morphology (Figure 5(c) and (d)). When the pH_2S was increased to 1.0 bar, some pyrite (FeS_2) appeared in addition to the pyrrhotite. Sporadic cubic pyrite crystals can be clearly seen on the surface of the pyrrhotite. Moreover, the thickness of the pyrrhotite crystals tended to increase compared with those formed at 0.50 bar H_2S. Only pure pyrite was identified when pH_2S increased to 2.0 bar, and the specimen surface was completely covered by large cubic pyrite crystals as shown in Figure 6(c) and (d). The cubic-like morphology of pyrite is consistent with its crystal structure and the literature.[22-25] In conclusion, the observed sequence of iron sulfide transformation with pH_2S was troilite → pyrrhotite → pyrrhotite/pyrite → pyrite, which is the same transformation order given in previous literature associated with temperature and time.[10,16] Iron sulfide transformed to more thermodynamically stable phases with increasing pH_2S.

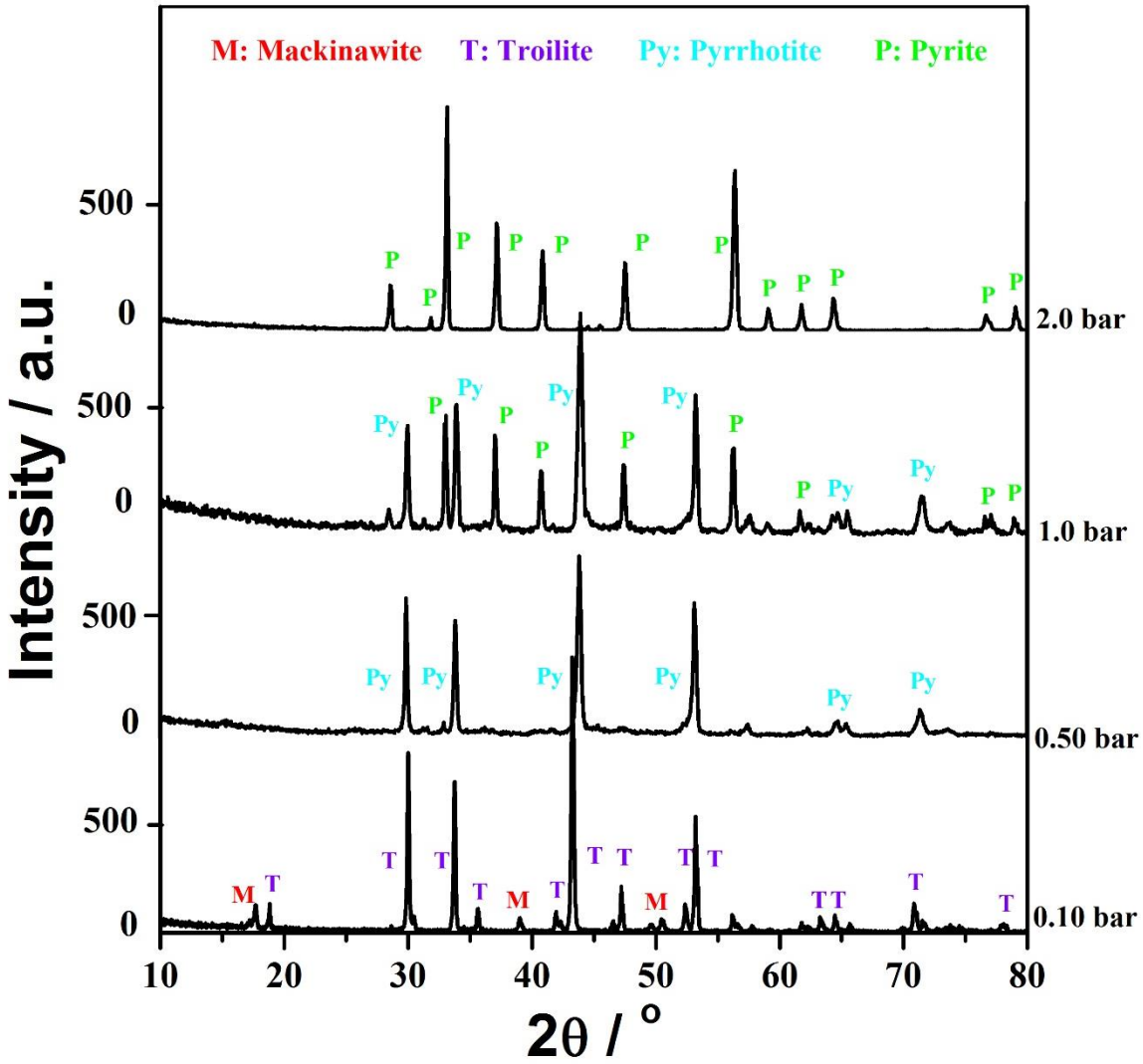

Figure 4. XRD patterns of corrosion products on the steel surface at different pH_2S, T=120°C, initial pH=4.0, 4 days.

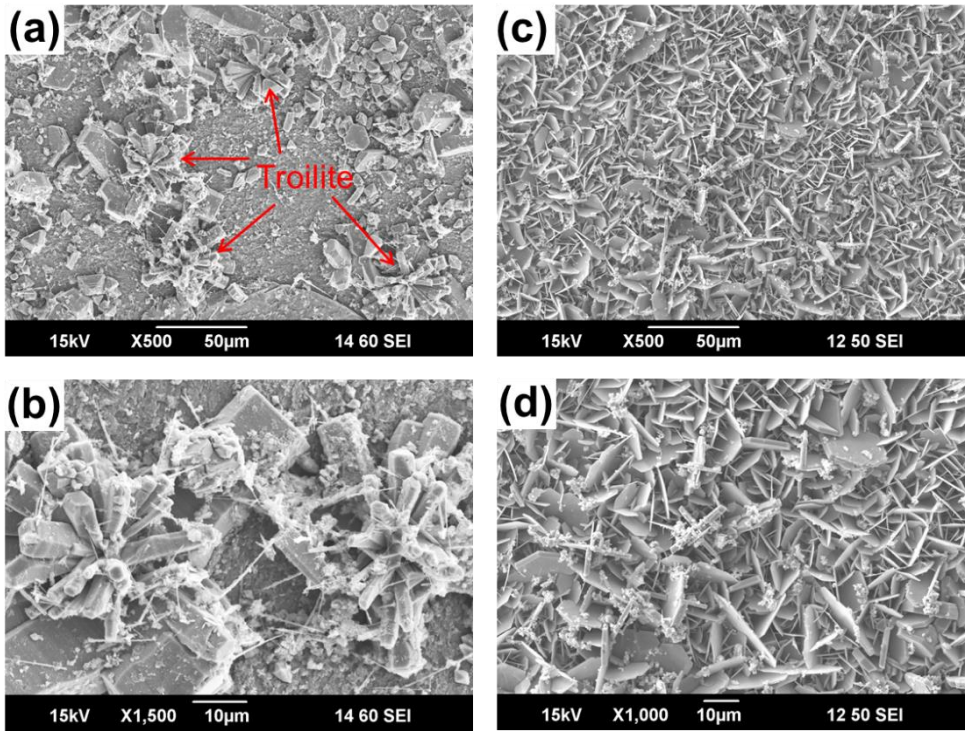

Figure 5. SEM morphologies: (a) and (b) troilite, pH_2S=0.10 bar, (c) and (d) pyrrhotite, pH_2S=0.10 bar, T=120°C, initial pH=4.0, 4 days.

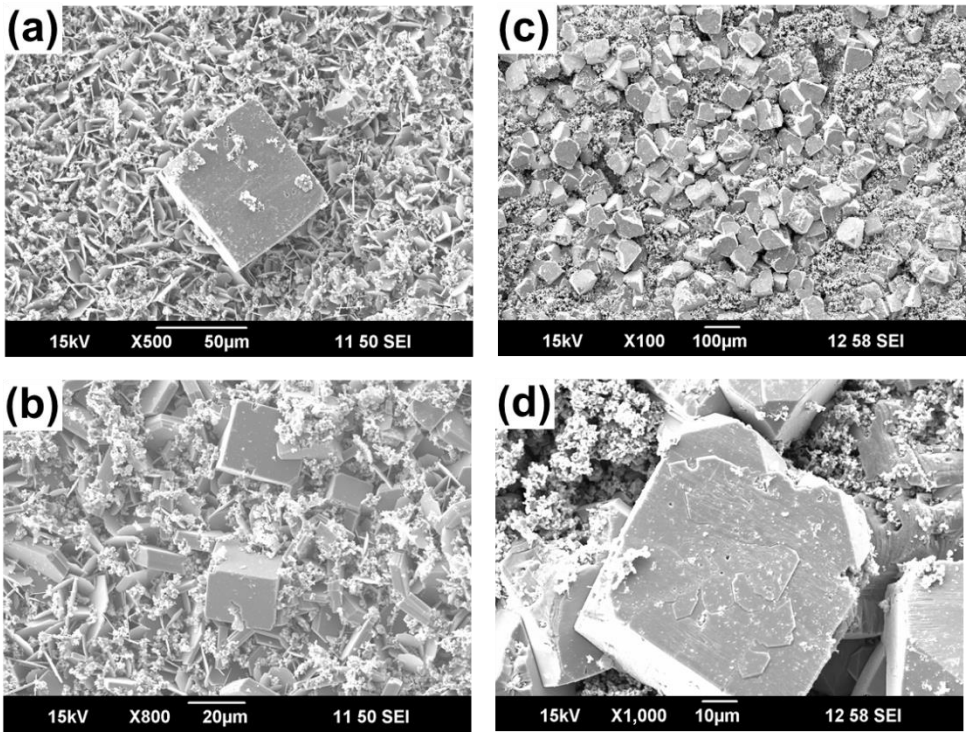

Figure 6. SEM morphologies: (a) and (b) pyrrhotite/pyrite, pH_2S=1.0 bar, (c) and (d) pyrite, pH_2S=2.0 bar, T=120°C, initial pH=4.0, 4 days.

At the end of each experiment, the autoclave was cooled down to ~ 50°C, then the Fe^{2+} and H_2S concentration were measured by a spectrophotometer and gas chromatography (GC), respectively. Then the corresponding parameters at the experimental condition (120°C) were back calculated. The

calculation details can be found in the previous publication.[16] The calculated results are summarized in Table 3, and were used as the inputs to generate Pourbaix diagrams based on an earlier version of the model[18] developed for lower temperature, as shown in Figure 7.

The vertical position of the arrow in each Pourbaix diagram represents the final experimental potential (potential range varied between -350 and -750 mV *vs.* SHE). The direction of the arrow represents the pH drift experienced during the test from initial pH 4.0 to the calculated values in Table 3. It can be seen that for all experiments the pH increased to around 5.4 during the 4-day experiments. For 0.10 and 0.50 bar pH_2S, the tip of the arrow, which represents the final experimental conditions, is right in the stability zone of pyrrhotite. At higher pH_2S (1.0 and 2.0 bar), the tip is right on the equilibrium line between pyrrhotite and pyrite, indicating the transformation between pyrrhotite and pyrite had an increased probability. The thermodynamic predictions are in good agreement with experimental results.

Table 3 Summary of the theoretical calculated final conditions at 120°C.

pH_2S, bar	Final Conditions at 120°C		
	pH_2S, bar	pH	Fe^{2+}, ppm
0.10	0.11	5.5	5.8
0.50	0.47	5.3	6.2
1.0	1.02	5.4	5.9
2.0	1.98	5.3	5.7

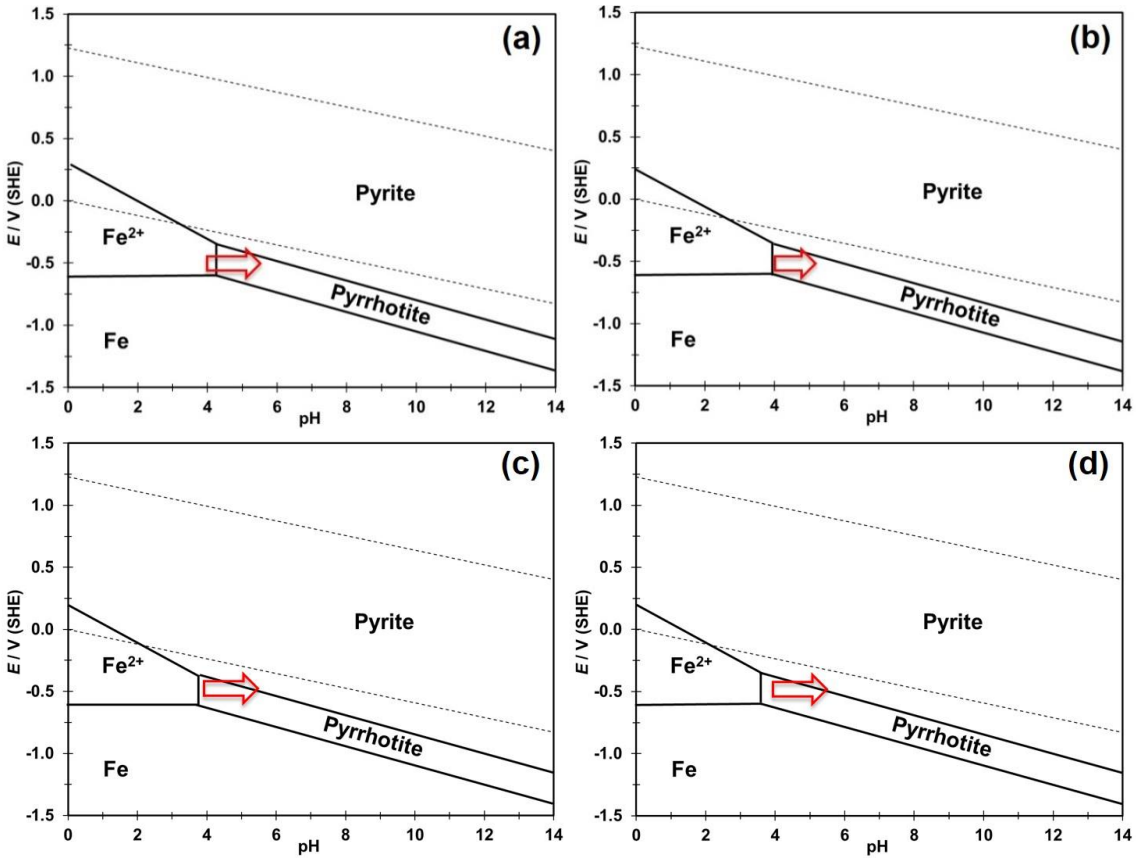

Figure 7. Pourbaix diagrams for Fe-H_2S-H_2O system by considering mackinawite/greigite/pyrrhotite/pyrite (a) pH_2S=0.10 bar, (b) pH_2S=0.50 bar, (c) pH_2S=1.0 bar, (d) pH_2S=2.0 bar, T=120°C, other input parameters are in Table 3.

Different iron sulfide layers have different effects on corrosion.[17] The steel surface was examined using profilometry after removing the corrosion product layers, as shown in Figure 8. For 0.10 bar and 0.50 bar H_2S, with troilite and pyrrhotite formation, the steel surfaces after removal of the corrosion product layer were relatively smooth. However, at higher pH_2S, severe localized corrosion occurred, coinciding with pyrite formation. From these images, the maximum calculated pit penetration rates are 6.2 mm/y and 10.1 mm/y at 1.0 bar and 2.0 bar pH_2S, respectively. This observation of localized corrosion associated with pyrite formation is consistent with previous research.[10,16,26]

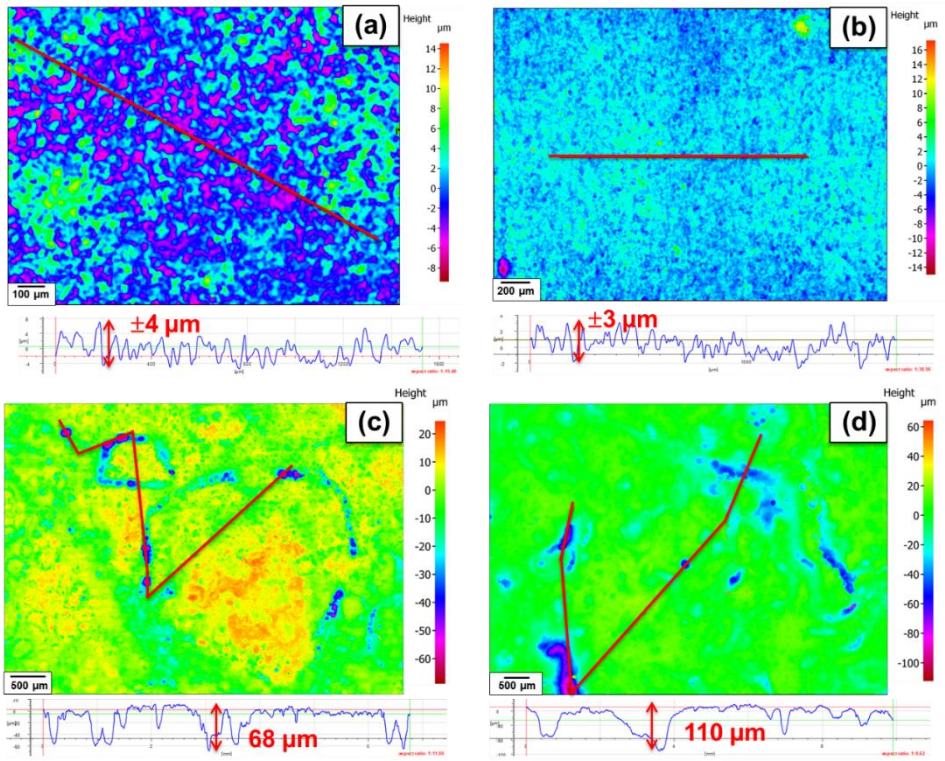

Figure 8. Surface profilometry after removing the corrosion products (a) 0.10 bar H_2S, troilite, (b) 0.50 bar H_2S, pyrrhotite, (c) 1.0 bar H_2S pyrrhotite/pyrite, (d) 2.0 bar H_2S, pyrite. T=120°C, initial pH=4.0, 4 days.

Does inner Fe_3O_4 layer eventually disappear?

The Fe_3O_4 layers obtained at different pH_2S values were examined via cross-section analysis. In this case, the XRD analysis could not identify the presence of Fe_3O_4 since the outer corrosion product layer was too thick or/and compact. The colors in Figure 9 qualitatively indicate the elemental composition of each layer. An inner iron oxide (Fe_3O_4) layer is clearly visible at every tested pH_2S. Focusing on the third column in Figure 9 for the oxygen element (which was used to indicate the location of the Fe_3O_4 layer), the thickness of Fe_3O_4 can be seen to decrease with increasing pH_2S.

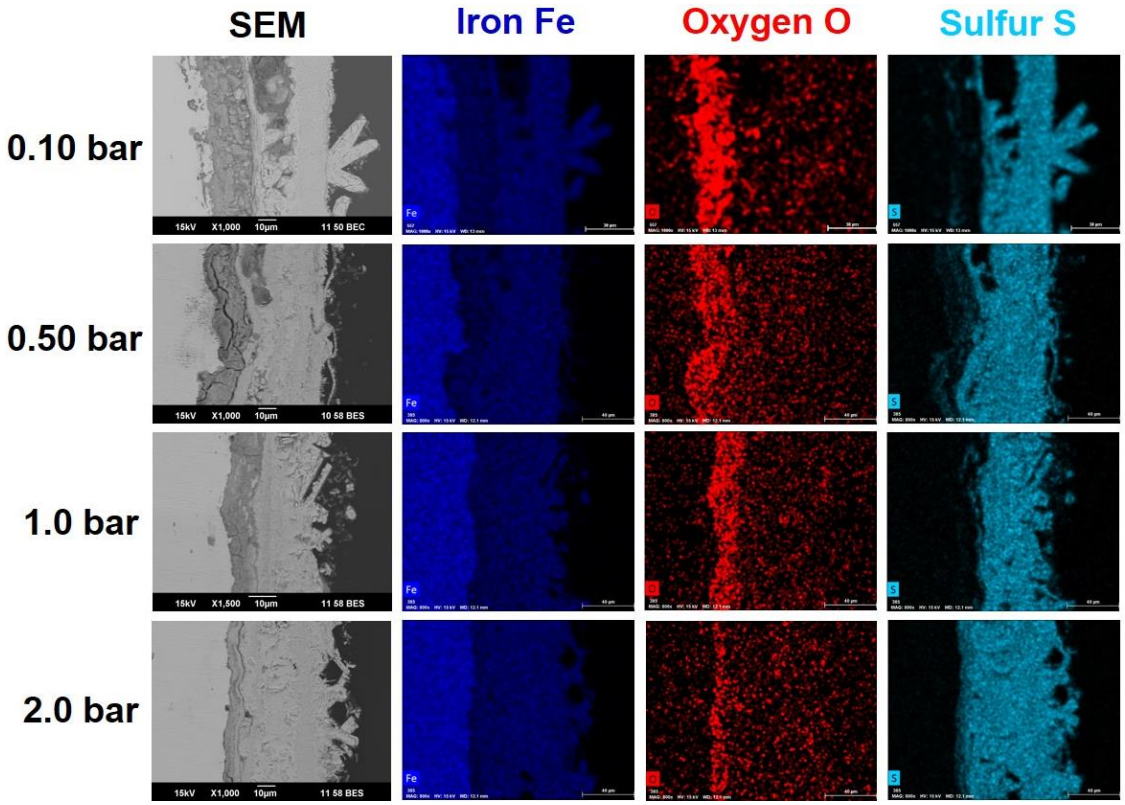

Figure 9. EDS mapping results for Fe, O and S distribution at different pH_2S, T=120°C, initial pH=4.0, 4 days.

With the increase of pH_2S, the thickness of Fe_3O_4 decreased from 25 µm to 5 µm. The average thickness of the Fe_3O_4 layer was measured and plotted in Figure 10. The results, again, demonstrate the existence of the conversion reaction, Equation (3), from Fe_3O_4 to iron sulfide. With more H_2S present in the solution as the reactant, more Fe_3O_4 was converted to iron sulfide. In addition, it is important to note that Fe_3O_4 did not completely convert and was still present even at 2.0 bar H_2S after the 4 day test.

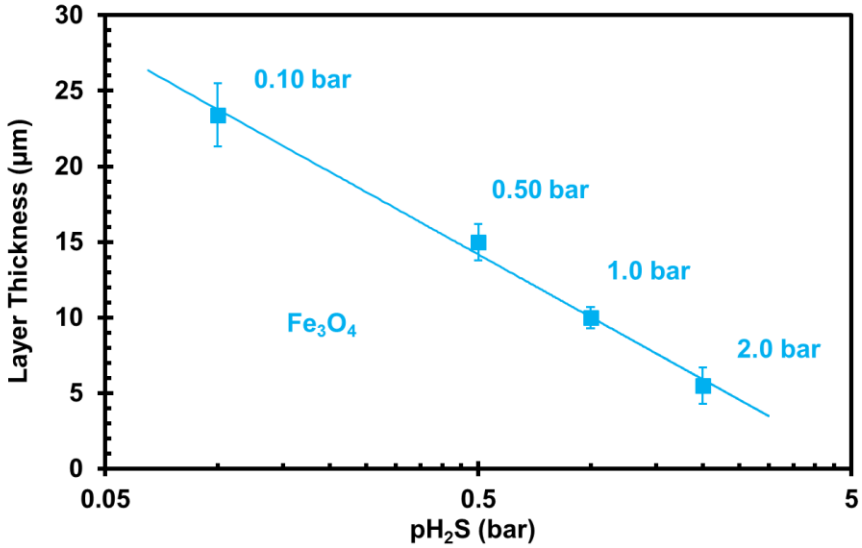

Figure 10. Layer thickness of Fe_3O_4 at different pH_2S, T=120°C, initial pH=4.0, 4 days.

Additional experiments at higher temperature (160°C), higher pH_2S (2.0 bar), and longer duration (21 days) were conducted to further confirm the above conclusion. These experimental parameters were expected to accelerate the conversion reaction, Equation (3). The cross-section and EDS mapping results are shown in Figure 11. It can be seen that Fe_3O_4 was still present as an inner layer (~ 15 µm) after 21 days exposure in 2.0 bar H_2S environment at 160°C. This result further demonstrated that Fe_3O_4 formed continuously at the steel surface even as a higher conversion rate was expected under these conditions (higher temperature and higher pH_2S). After a steady corrosion rate was reached, the Fe_3O_4 formation rate and conversion rate also became stable at an equivalent rate. Based on these results, it can be concluded that Fe_3O_4 I likely to be present as a corrosion product layer in the H_2S aqueous environments at high temperatures, although it is not predicted to be thermodynamically stable. Consequently, development of new mechanistic models for H_2S corrosion in the presence of iron sulfide corrosion product layers should also consider Fe_3O_4 since it seems to be ubiquitous and can influence the corrosion rate. [10,16]

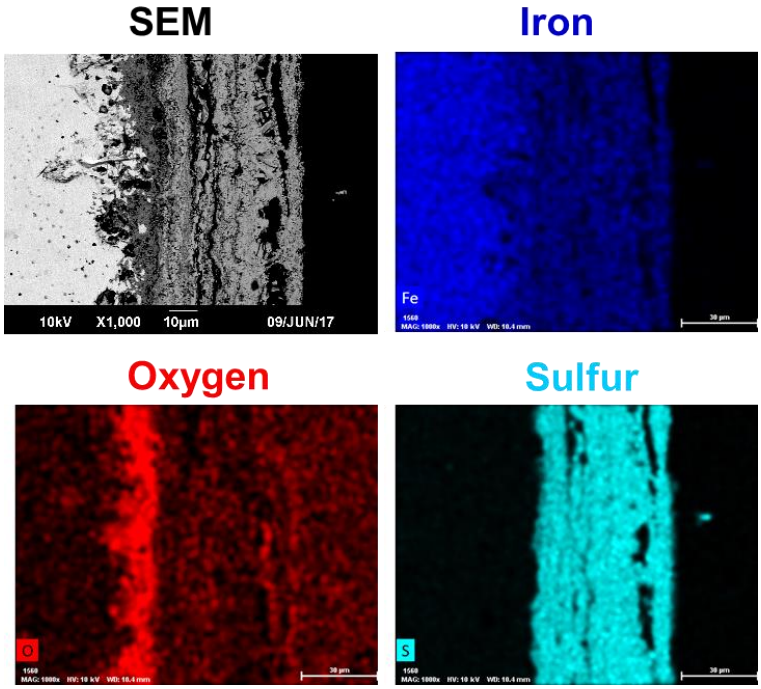

Figure 11. Cross-section and EDS mapping results for Fe, O and S distribution, T=160°C, pH_2S=2.0 bar, initial pH=4.0, 21 days.

A Modified Thermodynamic Model

A slightly modified Pourbaix diagram model, compared to the original work developed at lower temperature by Ning[18] is proposed here. For the prediction of iron sulfide layers, the Pourbaix diagram is identical to what Ning proposed since the thermodynamic data are valid up to 300°C.[10,16] Although the most thermodynamically stable forms of iron sulfide are pyrrhotite and pyrite, the user has the possibility to select any type of iron sulfides (mackinawite, troilite, pyrrhotite, and pyrite) and exclude others, because they are kinetically favored. Actually, the kinetics of conversion between the different iron sulfides is not well characterized and it is not possible, at this stage, to predict which phases or polymorphs will be actually present depending on the exposure time and other operating variables. This is an inherent issue, which was also present in Ning's research, when trying to predict kinetically favored phases (from experimental observations) using a thermodynamic (Pourbaix diagram) approach.

For the inner Fe_3O_4 layer, the proposed modification of the Pourbaix diagram is to keep the Fe_3O_4 stability region (Figure 12(a)) visible as a dashed zone in the Fe-H_2S-H_2O system, Pourbaix diagram (Figure

12(b)). This gives an indication that Fe_3O_4 is kinetically favored at high temperatures as part of the corrosion product layer near the metal surface. Considering only mackinawite as the iron sulfide corrosion product for simplicity, both Fe_3O_4 and mackinawite can form at 120°C under the operating conditions (represented by the red rectangle) according to Figure 12(c). Figure 12(d) shows that at low temperature, 25°C for example, the operating conditions are far away from the Fe_3O_4 formation region, so an inner Fe_3O_4 layer would not be expected.

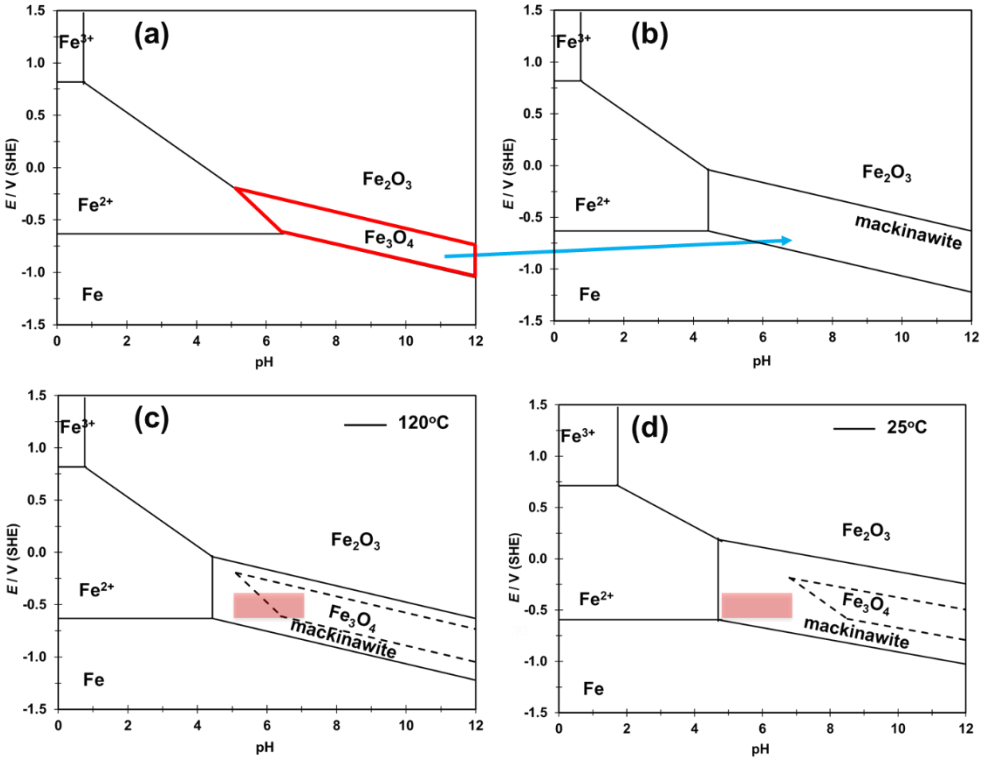

Figure 12. Pourbaix diagrams for (a) Fe-H_2S-H_2O system, 120°C; (b) Fe-H_2O system, 120°C; modified Pourbaix diagrams for Fe-H_2S-H_2O system (c) 120°C; (d) 25°C, 0.1 bar H_2S, [Fe^{2+}]=5 ppm, consider mackinawite only.

Figure 13(a) shows the modified Pourbaix diagram at 120°C by considering all the possible iron sulfides (mackinawite/troilite/greigite/pyrrhotite/pyrite). It can be seen that Fe_3O_4, pyrrhotite, and pyrite can form under the operating conditions, which is in good agreement with the above experimental results. Again, corrosion product predictions would not need to be modified at low temperature since the operating conditions are away from the Fe_3O_4 formation region, as shown in Figure 13(b).

The current modified Pourbaix diagram was also compared with two well-known software packages used in industry: Geochemist's Workbench (GWB) and OLI Corrosion Analyzer (OLI), as shown in Figure 13(c) and (d). It can be seen that GWB (using thermo.com.V8.R6+.dat) only predicts pyrrhotite formation and OLI only predicts FeS (unknown phase) and pyrite formation, neither of them has any indication of Fe_3O_4 formation. Again, these two models are thermodynamically sound and perfectly valid. However, the current modified Pourbaix diagram model would provide an indication of Fe_3O_4 formation at higher temperatures, which is very helpful for understanding corrosion mechanisms and corrosion product prediction with an increase in temperature.

However, it is important to point out that current study mainly focused on general corrosion, while the localized corrosion is the major concern in the industry field. The localized corrosion with pyrite formation and in the presence the inner Fe_3O_4 layer should be further investigated.

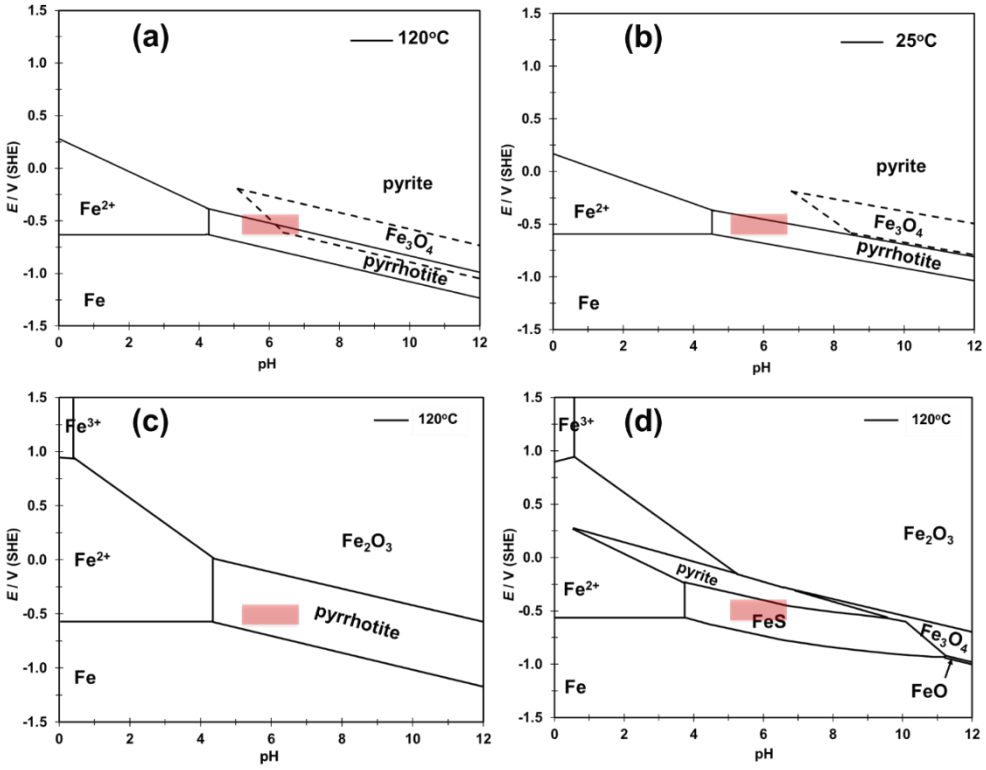

Figure 13. Modified Pourbaix diagrams for Fe-H_2S-H_2O system (a) 120°C; (b) 25°C; comparison Pourbaix diagrams for Fe-H_2S-H_2O system at 120°C generated by (c) the Geochemist's Workbench (GWB) based on thermo.com.V8.R6+.dat; (d) OLI Corrosion Analyzer (OLI), 0.1 bar H_2S, [Fe^{2+}]=5 ppm, consider mackinawite/troilite/greigite/pyrrhotite/pyrite.

CONCLUSIONS

The effect of pH_2S on corrosion kinetics and corrosion product layer transformation/conversion at high temperature was investigated. The main conclusions can be drawn as follows:

- The uniform corrosion rate tended to decrease with increasing pH_2S. Similar uniform corrosion behavior was observed in the presence of troilite and pyrrhotite. When pyrite formed, severe localized corrosion was observed.
- The observed iron sulfide formation and transformation with pH_2S at high temperature after 4 days is troilite (0.10 bar) → pyrrhotite (0.50 bar) → pyrrhotite/pyrite (1.0 bar) → pyrite (2.0 bar).
- The thickness of Fe_3O_4 decreased with increasing pH_2S, demonstrating a continuous process of Fe_3O_4 formation and conversion to iron sulfide. However, this thermodynamically less stable layer never completely converted and was always present in the tested conditions.
- A modified thermodynamic model (Pourbaix diagram) for high temperature H_2S corrosion was developed which shows a better agreement with the experiment results.

ACKNOWLEDGEMENTS

The author also would like to thank the following companies for their financial support: Anadarko, Baker Hughes, BP, Chevron, CNOOC, ConocoPhillips, DNV GL, ExxonMobil, M-I SWACO (Schlumberger), Multi-Chem (Halliburton), Occidental Oil Company, PTT, Saudi Aramco, SINOPEC (China Petroleum), and TOTAL.

REFERENCES

1. G. DeBruijin, “High-pressure, high-temperature technologies,” *Oilfield Review* 20, 3(2008): p. 46-60.
2. A. Shadravan, M. Amani, “HPHT 101-What Petroleum Engineers and Geoscientists Should Know About High Pressure High Temperature Wells Environment,” *Energy Science and Technology* 4, (2012): p. 36-60.
3. L. T. Popoola, A. S. Grema, G. K. Latinwo, B. Gutti, A. S. Balogun, “Corrosion problems during oil and gas production and its mitigation,” *International Journal of Industry Chemistry* 4, (2013): p. 46-35.
4. S. Gao, C. Dong, A. Fu, K. Xiao, X. Li, “Corrosion Behavior of the Expandable Tubular in Formation Water,” *International Journal of Minerals, Metallurgy, and Materials* 22, 2(2015): p. 149-156.
5. R. Feng, J. Beck, M. Ziomek-Moroz, S. N. Lvov, “High-Temperature Electrochemical Corrosion of Ultra-High Strength Carbon Steel in H_2S-Containing Alkaline Brines,” *Electrochimica Acta* 241, (2017): p. 341-352.
6. C. Dai, Y. Hu, “Fe (III) hydroxide nucleation and growth on quartz in the presence of Cu (II), Pb (II), and Cr (III): metal hydrolysis and adsorption,” *Environmental science & technology* 49, (2014): p. 292-300.
7. C. Dai, X. Zuo, B. Cao, Y. Hu, “Homogeneous and Heterogeneous $(Fe_x,Cr_{1-x})(OH)_3$ Precipitation: Implications for Cr Sequestration,” *Environmental science & technology* 50, (2016): p. 1741-1749.
8. J. Liu, C. Dai, Y. Hu, “Aqueous aggregation behavior of citric acid coated magnetite nanoparticles: effects of pH, cations, anions, and humic acid,” *Environmental research* 161, (2018): p. 49-60.
9. S. Gao, P. Jin, B. Brown, D. Young, S. Nesic, M. Singer, “Effect of High Temperature on the Aqueous H_2S Corrosion of Mild Steel,” *Corrosion* 73, 10 (2017): p. 1188-1191.
10. S. Gao, B. Brown, D. Young, S. Nesic, M. Singer, “Formation of Iron Oxide and Iron Sulfide at High Temperature and Their Effects on Corrosion,” *Corrosion Science* 135, (2018): p. 167-176.
11. W. Sun, D.V. Pugh, S. Ling, R.V. Reddy, J.L. Pacheco, R.S. Nisbet, N.M. Nor, M.S. Kersey, L. Morshidi, “Understanding and Quantifying Corrosion of L80 Carbon Steel,” CORROSION/2011, paper no. 11063 (Houston, TX: NACE, 2011).
12. J.S. Smith, J.D. Miller, “Nature of sulfides and their corrosive effect on ferrous metals: a review,” *British Corrosion Journal* 10, 3(1975): p. 136-143.
13. I.H. Omar, Y.M. Gunaltun, J. Kvarekval, A. Dugstad, “H_2S corrosion of carbon steel under simulated kashagan field conditions,” CORROSION/2005, paper no. 05300 (Houston, TX: NACE, 2005).
14. J. Banas, U. Lelek-Borkowska, B. Mazurkiewicz, W. Solarski, “Effect of CO_2 and H_2S on the composition and stability of passive film on iron alloys in geothermal water,” *Electrochimica Acta* 52, (2007): p. 5704-5714.
15. W. Sun, D.V. Pugh, S.N. Smith, S. Ling, J.L. Pacheco, R.J. Franco, “A parametric study of sour corrosion of carbon steel,” CORROSION/2010, paper no. 10278 (Houston, TX: NACE, 2010).
16. S. Gao, P. Jin, B. Brown, D. Young, S. Nesic, M. Singer, “Corrosion Behavior of Mild Steel in Sour Environments at Elevated Temperatures,” *Corrosion* 73, 8(2017): p. 915-926.
17. S. Gao, B. Brown, D. Young, S. Nesic, M. Singer, “Formation Mechanisms of Iron Oxide and Iron Sulfide at High Temperature in Aqueous H_2S Corrosion Environment,” *Journal of The Electrochemical Society* 163, 3(2018): p. C171-C179.
18. J. Ning, Y. Zheng, B Brown, D Young, S Nesic, M Singer, “A Thermodynamic Model for the Prediction of Mild Steel Corrosion Products in an Aqueous Hydrogen Sulfide Environment,” *Corrosion* 71, (2015): p. 945-960.
19. Y.R. Thodla, F. Gui, K. Evans, C. Joia, I.P. Baptista, “Corrosion Fatigue Performance of Super 13 CR, Duplex 2205 and 2507 for Riser Applications,” CORROSION/2010, paper No. 312 (Houston, TX: NACE, 2010).
20. M. Singer, A. Camacho, B. Brown, S. Nesic, “Sour Top-of-the-Line Corrosion in the Presence of Acetic Acid,” *Corrosion* 67, (2011): p. 085003-1-085003-16.
21. P. Bai, S. Zheng, C. Chen, H. Zhao, “Investigation of the Iron–Sulfide Phase Transformation in Nanoscale,” *Crystal Growth & Design* 14, (2014): p. 4295-4302.
22. P. Bai, S. Zheng, H. Zhao, Y. Ding, J. Wu, C. Chen, “Investigations of the diverse corrosion products on steel in a hydrogen sulfide environment,” *Corrosion Science* 87, (2014): p. 397-406.

23. B. Yuan, W. Luan, S. Tu, J. Wu, “One-step synthesis of pure pyrite FeS_2 with different morphologies in water,” *New Journal of Chemistry* 39, (2015): p. 3571-3577.
24. Y. Liang, P. Bai, J. Zhou, T. Wang, B. Luo, S. Zheng, “An efficient precursor to synthesize various FeS_2 nanostructures via a simple hydrothermal synthesis method,” *CrystEngComm* 18, (2016): p. 6262-6271.
25. H. Xian, J. Zhu, X. Liang, H. He, “Morphology controllable syntheses of micro- and nano-iron pyrite mono- and poly-crystals: a review,” *RSC Advances* 6, (2016): p. 31988-31999.
26. J. Ning, Y. Zheng, B. Brown, D. Young, S. Nesic, “The Role of Iron Sulfide Polymorphism in Localized H_2S Corrosion of Mild Steel,” *Corrosion* 73, (2017): p.155-168.